

Extensive air showers accompanied by γ -ray families with $\sum E_{\gamma,H} \geq 10$ TeV and general extensive air showers

Y. Fukushima, C. Hamayasu, T. Mitsumune, To. Saito, M. Sakata,
M. Shima, and Y. Yamamoto

Department of Physics, Konan University, Kobe, Japan

S. Dake and M. Kawamoto

Department of Physics, Kobe University, Kobe, Japan

M. Kusunose and N. Ohmori

Department of Physics, Kochi University, Kochi, Japan

K. Kasahara

Institute of Cosmic Ray Research, University of Tokyo, Tanashi, Tokyo, Japan

T. Shirai and S. Torii

Faculty of Engineering, Kanagawa University, Yokohama, Japan

N. Hotta

Department of Physics, Faculty of Education, Utsunomiya University, Utsunomiya, Japan

(Received 6 June 1988; revised manuscript received 12 October 1988)

Extensive air showers (EAS's) accompanied by families of high-energy cascade showers were observed at Mt. Norikura (738 g cm^{-2}). 99 families of γ -ray- and hadron-origin showers with total energies $\sum E_{\gamma,H} \geq 10$ TeV were obtained. The success rate of the combination between families and EAS's reaches to almost 90% (87 events). The families are associated with young EAS's, with mean age parameter $s \sim 0.7$, whose sizes distribute widely over three orders of magnitude up to 10^8 . The size spectrum of the family-associated EAS's coincides with the general EAS's in the size region above 5×10^6 but the former drops rapidly from the latter below this critical size. From the absolute intensity of $\sum E_{\gamma,H}$ spectrum the proton fraction in the primary cosmic rays is deduced to be $(14 \pm 5)\%$, with an error of one standard deviation, in the primary energies $(5 \times 10^{14}) - 10^{16}$ eV, in comparison with a Monte Carlo simulation assuming an adequate interaction model. This agrees with the result obtained by the work with other mountain data and is also compatible with the result inferred from the size spectrum gap between the family-associated EAS's and the general EAS's in the region below the critical size.

I. INTRODUCTION

A simultaneous observation of γ -ray and hadronic families and extensive air showers (EAS's) gives us more information than that obtained by separate observations of EAS's and families and is more sensitive to the study for the particle interaction and for the chemical composition of primary cosmic-ray particles. This thought has caused the planning and performance of experiments with hybrid installations.

The first experiment with a combination of an emul-

sion chamber and an EAS array consisting of Čerenkov counters, spark chambers, and scintillation counters was carried out by Smorodin *et al.*¹ at an airplane altitude in the early 1960s. The second experiment was started by Dake *et al.*² at Mt. Norikura (738 g cm^{-2}) in 1968 and also started by Matano *et al.*³ at sea level and continued at Mt. Chacaltaya in 1975. The experiment with a 18-m^2 spark-chamber array, 50 scintillation counters, and 6.4-m^2 emulsion chambers was carried out by Dake *et al.*⁴ at Mt. Norikura in 1971. With the data of this experiment, a large- p_t study of EAS subcores accompanied by γ -ray

families was done by Sakata *et al.*,⁵ and also the mean p_t value of secondary pions against the EAS axis was deduced by Munakata *et al.*⁶ from the lateral distribution of γ rays.

With the availability of CERN $S\bar{p}pS$ collider data on phenomenological properties of particle production up to 4.0×10^{14} eV in the laboratory system,⁷ one may reasonably extrapolate these properties up to higher energies involved in our cosmic-ray studies, up to 10^{16} eV. New results from the Fermilab Tevatron collider will provide experimental data up to 2×10^{15} eV to check this extrapolation. The hadron-nucleus interaction in the atmosphere is not exactly equivalent to the simple superposition of the hadron-hadron interaction. The rapidity distribution of secondary particles is, however, considered to be not so different from that of the hadron-hadron interaction in the fragmentation region from which the high-energy families emerge out. Therefore, an adequate Monte Carlo simulation using the available data obtained by accelerators and cosmic-ray experiments makes it possible to infer the fraction of primary protons from the experimental data of high-energy families and of EAS's accompanied by families in the energy region around the so-called "knee" of the primary spectrum.

This paper describes the results obtained in the combined experiments performed at Mt. Norikura in 1980 and 1981 and in 1985. The air-shower array and the emulsion and/or x-ray film (EX) chamber was used in the same setup in these experiments except for a few new-type burst detectors⁸ in 1985. The experiment gives the integral spectrum of total family energy $\sum E_{\gamma,H}$, which means the sum of γ -ray energy and electromagnetic energy released by hadronic jets in the EX chamber. From the comparison of the family intensity at $\sum E_{\gamma,H} \geq 15$ TeV with that of a Monte Carlo simulation is given a fraction of primary protons averaged over a wide energy range around 10^{15} eV. The integral size spectrum is also given for both the general EAS's and the family-associated EAS's. The intensity gap between them seen in the smaller side of a critical size, beyond which they coincide with each other, is sensitively affected by the fraction of primary protons which must have the highest generation rate of such families at mountain altitudes. When this intensity gap is compared with the simulation result at the designated shower size, it is possible to estimate a fraction of protons in a much narrower energy range.

II. EXPERIMENTAL ARRANGEMENT AND PROCEDURE

The experimental apparatus consists of a scintillation-counter array (32 channels of 0.25 m^2 unit area) for EAS density, a 54-m^2 spark-chamber array as a core detector, a 20-m^2 iron EX chamber for detection of families settled under the spark-chamber area, and a burst scintillation-counter array (72 channels with 0.25 m^2 unit area) to measure the burst size just beneath the iron EX chamber.

Figures 1 and 2 show the plan view of the EAS array and the side view of the central arrangement of detectors, respectively. The EAS data were taken with two kinds of triggers. One was a burst trigger under the iron EX

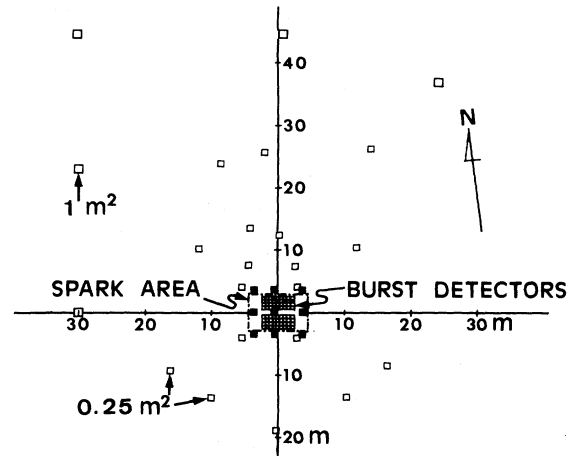


FIG. 1. Map of the EAS scintillation-counter array. Nine scintillation counters marked by closed squares are used for the air-shower trigger.

chamber when at least one of 72 burst detectors gave a response bigger than about 2000 particles per detector (0.25 m^2 unit), whose trigger frequency was about 40 events per day. Another one was an air-shower (AS) trigger by any one of four sets of fourfold coincidence with 50 particles/ 0.25 m^2 each out of nine central non-covered scintillation counters settled beside the EX chamber. The frequency of the AS trigger was about 25 events per day. The live time of recording system of EAS data, including burst data, was 95.7% (289.5 days) in 1980 and 1981 and 98.4% (251.2 days) in 1985. The arrival directions of air showers, which are indispensable for combining them with families, were measured by four sets of spark chambers suspended from the ceiling as shown in Fig. 2.

The live time of the spark-chamber system was a little higher than 80% (1980 and 1981) and 90% (1985), respectively. The shower size N_e and age parameter s of EAS's were determined by fitting the NKG function⁹ with the Molière unit of 110 m to the density data in the core distance from 3 to 40 m. Using the experimental results¹⁰ about the transition effect of EAS shower-particle density for thin materials, the corrections were made on

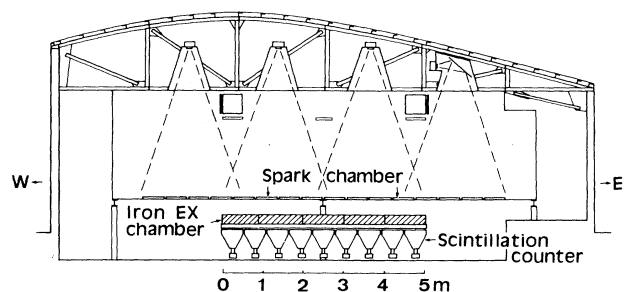


FIG. 2. Side view of the arrangement of the central hybrid installations.

N_e and s for the response excesses in the case of a 3-cm-thick plastic scintillator and for the transition effects due to the cover, roof, and ceiling materials. As a result, s was increased by an amount of 0.18–0.16 and N_e was multiplied by a factor of 0.65–1.16 depending on the uncorrected values of s from 0.4 to 1.2, respectively.

The design of the iron EX chamber is illustrated in Fig. 3. The photosensitive layers are mainly composed of Sakura cosmic-ray-type x-ray films. The emulsion plates are put in three layers of a part (4 m^2) of the chamber for the calibration of cascade-shower energy. In order to get the shower energy by the darkness of x-ray films it was calibrated by counting the number of shower tracks sketched carefully from the emulsion plates. The total thickness of iron is 26 cm, i.e., 14.5 radiation length (r.l.) and about 1.4 mean free path for nucleons. In this chamber the cascade showers started before 10 r.l. are easily found, but it is hard to find out the showers started after 10 r.l. because of insufficient cascade development in the residual part of the EX chamber, except for very-high-energy ones. Then, all γ -ray-origin showers and some of hadron-origin ones (about $\frac{2}{3}$ of the nucleons and about half of the pions) above a threshold energy are detected. A clear distinction between these two kinds of showers is impossible for a significant fraction of cascade showers. Then, we dare not distinguish them individually.

III. CASCADE SHOWERS AND THEIR FAMILY

Figure 4 shows the integral energy spectrum of cascade showers, which consists of all isolated cascade showers without any companions and the top energy shower in each family. The data were obtained from the emulsion chambers of 4 m^2 in 1980 and 1981 and of 5 m^2 in 1985. These spectra are both represented by a simple power -1.95 and their intensities coincide with each other only within a few percent difference. The detection threshold energy for cascade showers on x-ray films is 3.0 TeV in 1980 and 1981 and 4.0 TeV in 1985.

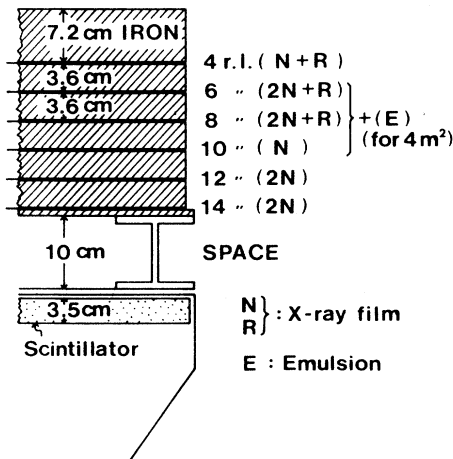


FIG. 3. Configuration of the EX chamber and the burst detector.

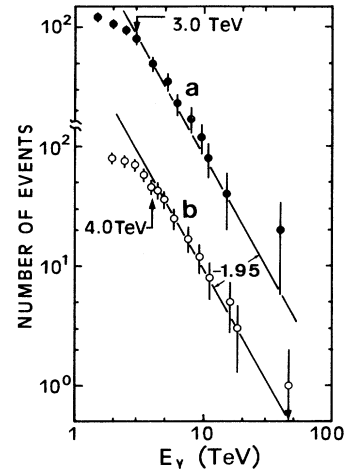


FIG. 4. Integral energy spectrum of the single cascade showers obtained in 1980 and 1981 (a) in 1985 (b). For family events, only a top energy cascade shower is used.

Figure 5 shows the zenith-angle distributions of families with total energy $\sum E_{\gamma,H} \geq 10 \text{ TeV}$ for $n_{\gamma,H} \geq 2$ with the minimum energy $E_{\min} = 3 \text{ TeV}$, where $n_{\gamma,H}$ is the number of γ rays and hadron-origin showers in a family. They are consistent with each other for both data obtained in 1980 and 1981 and in 1985 and are well represented by the theoretical curve with $x_0/\Lambda_{\text{att}} = 7.5 \pm 0.5$. The value $\Lambda_{\text{att}} = 98 \pm 7 \text{ g cm}^{-2}$ thus obtained for $x_0 = 738 \text{ g cm}^{-2}$ is consistent with the other mountain EX chamber data.^{11–14} The integral $\sum E_{\gamma,H}$ spectrum of families, found in all areas of the EX chamber, is shown in Fig. 6, where E_{\min} is also taken to be 3.0 TeV. A few small cascade showers with energies between 3.0 and 4.0 TeV may be missed in the 1985 data. The bending of the $\sum E_{\gamma,H}$ spectrum at 13 TeV in the 1985 data (open circles) is considered to be due to this effect. These spectra are both represented by a power -1.3 . The solid curves

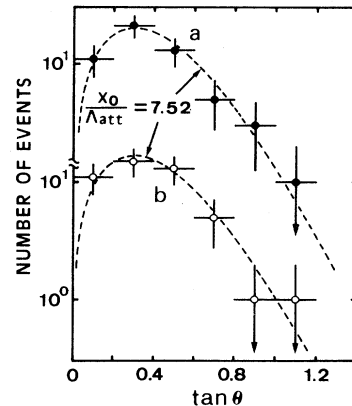


FIG. 5. Zenith-angle distribution of families with $\sum E_{\gamma,H} \geq 10 \text{ TeV}$, $n_{\gamma,H} \geq 2$ for $E_{\min} = 3.0 \text{ TeV}$. The distributions obtained in 1980 and 1981 (a) and in 1985 (b) are both consistent with the theoretical curve of $x_0/\Lambda_{\text{att}} = 7.52$ ($\Lambda_{\text{att}} = 98.1 \text{ g cm}^{-2}$).

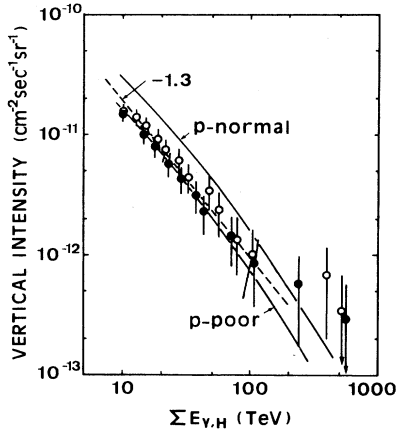


FIG. 6. Integral $\Sigma E_{\gamma,H}$ spectrum of the families for $n_{\gamma,H} \geq 2$ and $E_{\min} = 3$ TeV. The data are obtained from all areas of the EX chambers in 1980 and 1981 (closed circles) and in 1985 (open circles). The errors are statistical ones only. The solid curves are the simulation results of p -normal and p -poor models.

indicate the results of a Monte Carlo simulation¹⁵ calculated for two typical models, p -normal and p -poor ones, in the primary chemical composition whose details are given in Table I. In the nuclear interaction model we adopt a rising cross section proportional to $E^{0.055}$ for the p -air-nucleus inelastic collision. To save the calculation time, the simulation given here was carried out by neglecting all shower particles with energies less than 1 TeV, but it includes the contribution of the primary particles till the minimum energy, 40 TeV, in the primary spectrum.

Interpolating the curves for two composition models with the assumed proton fractions, about 13% (p -poor) and 35% (p -normal), the absolute intensity of the experimental $\Sigma E_{\gamma,H}$ spectrum, in the range $\Sigma E_{\gamma,H} \geq 15$ TeV, gives the proton fraction ($14 \pm 5\%$) in a wide range of the primary particle energies, (5×10^{14})– 10^{16} eV. The error, $\pm 5\%$ of one standard deviation (1σ), involves the statistical ones in both the experiment and the simulation and also involves an error in the experiment arising from the ambiguity in the attenuation length Λ_{att} . There is also involved a rather big ambiguity, $\pm 8.5\%$ in 1σ , in the ener-

gy calibration of cascade showers, which makes about $\pm 13\%$ error in the absolute intensity of the $\Sigma E_{\gamma,H}$ spectrum and also makes $\pm 3\%$ error in the proton fraction. The above obtained value of the proton fraction is consistent with the result of 15–20%, obtained by Ren *et al.*¹⁶ with the EX chamber data at Mt. Fuji and Mt. Kanbala.

Figure 7 shows the altitude dependence of the vertical intensity of families with $E_{\min} = 4.0$ TeV. The data at Mt. Kanbala and Mt. Fuji are obtained by the lead EX chambers, where the cascade showers started at depths deeper than 6 r.l. from the chamber top and the showers with successive interactions are both omitted as the hadron-origin ones. For comparison with the data obtained by the lead EX chambers, the same selection rules are applied to our analysis. The data indicated by the open circles and open triangles in this figure are ones after a correction, due to a difference of the mean free path of hadrons in lead (~ 30 r.l.) and iron (~ 10 r.l.), on our data obtained by the iron EX chamber. This is made with the help of the hadron flux data obtained by the iron thick EX chamber exposed at Mt. Fuji.¹⁷ The curves in this figure are the theoretical ones¹⁸ for $\Lambda_{\text{att}} = 100$ g cm⁻² (solid curves) and 110 g cm⁻² (dashed curves). The experimental data agree with the theoretical curves of $\Lambda_{\text{att}} = 100$ g cm⁻², within statistical errors, which is consistent with the above value derived from the zenith-angle distribution of families.

IV. FAMILY-ASSOCIATED EAS's AND GENERAL EAS's

A. Method of combination between families and EAS's

Here is described the procedure of the combination between families found in the EX chamber and EAS's triggered by large bursts. Every family is always situated just at the position of the detector giving the maximum burst in each EAS. So, we list about 15 EAS events with large bursts from the largest one in each burst detector. Then, we check whether or not each large burst event is identified with one of families located in a zone of the EX chamber just above the burst detector. The combination between EAS and family is carried out by satisfaction of the following three conditions: (i) coincidence of projected components of arrival angles within 3° which corre-

TABLE I. Assumed primary chemical compositions (in percent) in the integral energy spectrum.

Primary energy		$\geq 5 \times 10^{14}$	$\geq 10^{15}$	$\geq 2 \times 10^{15}$	$\geq 4 \times 10^{15}$
E_0 (eV)					
p -poor	p	16.7	14.5	12.9	11.9
	He	9.2	8.2	7.4	6.9
	Fe	42.5	46.3	49.4	51.5
	Others	31.6	31.0	30.3	29.7
p -normal	p	35.5	35.4	35.1	35.0
	He	15.1	13.9	13.0	12.0
	Fe	3.8	3.2	2.8	2.5
	Others	45.6	47.5	49.1	50.5

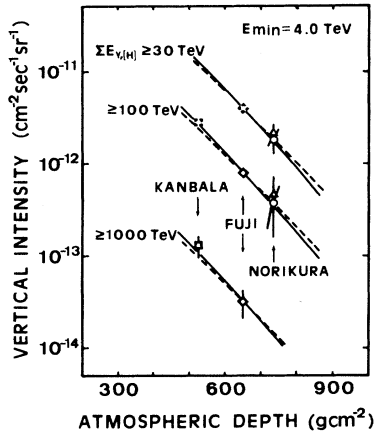


FIG. 7. Atmospheric-depth dependence of the vertical intensities of families. The data obtained in the iron EX chamber are transformed to the connected ones indicated by open circles (1980 and 1981) and open triangles (1985) for the lead EX chamber to compare with the data at Mt. Kanbala and Mt. Fuji. The data points of 30 TeV at Mt. Fuji and 100 TeV at Mt. Kanbala are both extrapolations from higher-energy regions.

sponds to the error in the roughly determined direction by spark-chamber photographs; (ii) coincidence of location within a radius of about 10 cm which corresponds to the experimental error of burst-peak position determined from equidensity contours on the burst density map; (iii) the observed maximum burst density (particles/0.25 m²) should be more than, but consistent with, the number of electrons under the EX chamber which is estimated from the cascade showers in the family under approximation B of the cascade-shower theory.

The third condition was required because there is usually a significant contribution to the burst density from the cascade showers of low-energy air-shower particles, especially from the hadron-origin ones, with energy less than the detection threshold of the EX chamber. This contribution increases as the EAS size increases. With the spark-chamber photographs the combination thus decided was often confirmed by finding a local spark density peak at the position corresponding to the family within several centimeters. As a result 170 EAS events in 1980 and 1981 and 115 EAS events in 1985 were combined with families with energy greater than 1 TeV. Most parts of single cascade-shower events in 1985 are not combined because they are not considered to have any essential role in our present analysis. In these EX chambers we found 53 families (1980 and 1981) and 46 families (1985) with total energy $\sum E_{\gamma,H} \geq 10$ TeV for $n_{\gamma,H} \geq 2$ under the condition $E_{\min} = 3$ TeV. Out of them, 44 families (1980 and 1981) and 43 families (1985) were combined with EAS's, and the rate of combination reached 83.0% and 93.5%, respectively. The reason why some families are out of the combination arises from the dead time of the spark chambers measuring the arrival direction of EAS's and also from the dead time of the recording system of EAS data which was 4.3% (1980 and 1981) and 1.6% (1985) of the total running time.

In Fig. 8 is shown the scatter diagram of $N_e - \sum E_{\gamma,H}$ correlation of those combined events with $\sum E_{\gamma,H} \geq 10$ TeV for $n_{\gamma,H} \geq 3$ (open circles) and $n_{\gamma,H} = 2$ (solid circles) with $E_{\min} = 3.0$ TeV. There is one event with very small size in the 1980 and 1981 data (a) and a few large EAS events in the 1985 data (b). Except for them, both distributions are very similar to each other and we can say that the EAS accompanied by families with $E_{\gamma,H} \geq 10$ TeV distribute widely in the size range more than 3 orders of magnitude.

B. Zenith-angle distribution and attenuation of general EAS's

First, we describe the way of the event selection of general EAS's taken by the AS trigger. We employed the EAS data recorded under the stable experimental conditions, especially for the trigger level, during 170 days in 1980 and 1981 and 220 days in 1985. The preliminary values of N_e and s were obtained by the iteration process of fitting the NKG lateral function under the assumption of vertical incidence. First, we pick up the EAS whose preliminary sizes are larger than 1.4×10^6 and whose shower axes hit the area within the circle of radius 7 m from the array center. Second, we measure their arrival angles from the spark-chamber photographs. Then, the shower size, age parameter, and the axis location are recalculated. Figures 9(a) and 9(b) show the maps of axis location of the general EAS with sizes larger than the recalculated size 2×10^6 for the 1980 and 1981 data and for the 1985 data, respectively. The events in the circle of radius 5 m, where the distributions are considered to be nearly uniform, are used in the present analysis.

In order to get the vertical intensity of EAS's it is necessary to know the zenith-angle distribution. Figure 10 shows the ones for 87 EAS events accompanied by families (a) and for the general EAS with sizes larger than 2×10^6 (b), which are both the sum of the data obtained in 1980 and 1981 and in 1985. It is reasonable that the zenith-angle distribution of the family-associated EAS's, which is represented by the theoretical curve with $x_0/\Lambda_{\text{att}} = 7.4 \pm 0.6$, is almost the same as the family's one shown in Fig. 5. However, the zenith-angle distribution

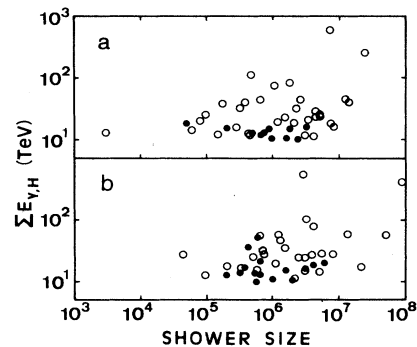


FIG. 8. Scatter diagram of $N_e - \sum E_{\gamma,H}$ for the EAS's accompanied by families with $\sum E_{\gamma,H} \geq 10$ TeV, obtained in 1980 and 1981 (a) and in 1985 (b). Open and solid circles indicate the families with $n_{\gamma,H} \geq 3$ and $n_{\gamma,H} = 2$, respectively.

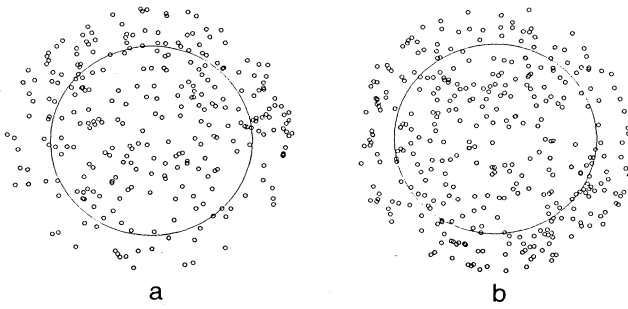


FIG. 9. Location maps of shower axes of the general EAS's with $N_e \geq 2 \times 10^6$ obtained in 1980 and 1981 (a) and in 1985 (b). Only the events in the circle of radius 5 m are used for the size spectrum.

of the general EAS's, which is represented by $x_0/\Lambda_{\text{att}} = 6.2 \pm 0.4$, is somewhat flatter than the associated EAS's. This difference can be explained by the fact that the general EAS's include some inclined EAS's with somewhat big age parameters, which are not surely accompanied by high-energy families. As a result the attenuation length of the frequency of EAS's is given by $\Lambda_{\text{att}} = 120 \pm 7 \text{ g cm}^{-2}$ at the shower size around 2×10^6 for the general EAS's at the atmospheric depth 738 g cm^{-2} .

Figure 11 shows the atmospheric-depth dependence of the absolute intensity of the general EAS's for $N_e \geq 10^6$. The experimental data obtained by several groups at mountain altitudes, i.e., Bolivian Air Shower Joint Experiment (BASJE) at Mt. Chacaltaya,¹⁹ Tien Shan,²⁰ Osaka City University (OCU)^{21,22} at Mt. Norikura, and Akeno,²³ and at sea level, i.e., Moscow,²⁴ Tokyo Institute for Nuclear Study (INS),²⁵ Kobe,²⁶ Lodz,²⁷ and Durham²⁸ are summarized in this figure. The present data indicated by a cross in an open circle show a good consistency with other experimental data. The slope of the straight line connecting our data and the Akeno data in

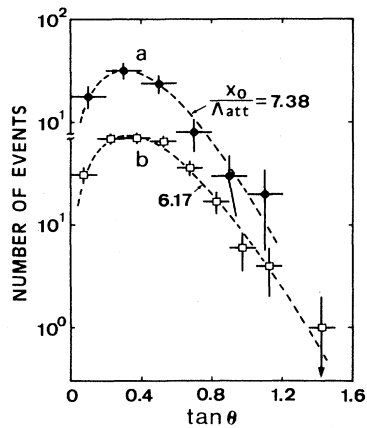


FIG. 10. Zenith-angle distribution of the 87 EAS events accompanied by families with $\sum E_{\gamma,H} \geq 10 \text{ TeV}$ (a) and of the general EAS's with $N_e \geq 2 \times 10^6$ (b) which are both the sum of the data obtained in 1980 and 1981 and in 1985. Curves are the best fit theoretical ones.

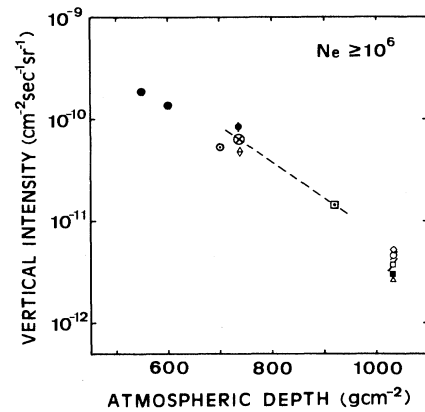


FIG. 11. Atmospheric-depth dependence of vertical intensity of EAS's at the size 10^6 . The mountain level data are Chacaltaya (\bullet), Tien Shan (\odot), OCU data (\bullet and \diamond), and our present data (\otimes) at Norikura and Akeno (\square). The sea-level data are Moscow (\diamond), Lodz (\square), Tokyo INS (\circ), Kobe (\blacksquare), and Durham (\triangle). The dashed line connecting our data and the Akeno data has an attenuation length $\Lambda_{\text{att}} = 122 \text{ g cm}^{-2}$.

which the same type scintillation counters as ours are used is given by $\Lambda_{\text{att}} = 122 \text{ g cm}^{-2}$. This value agrees with the attenuation length $\Lambda_{\text{att}} = 120 \pm 7 \text{ g cm}^{-2}$ obtained above from the zenith-angle distribution of the general EAS's.

C. Size spectra of EAS's with families and of general EAS's

Clear differences between the EAS's accompanied by families and the general EAS's are in the size dependence of the mean age parameter and also in the size spectrum itself.

Figure 12 shows the size dependence of age parameter s determined in the lateral range of 3–40 m from the shower axis. The closed circles indicate the mean age parameter in each size bin for the family-associated EAS's,

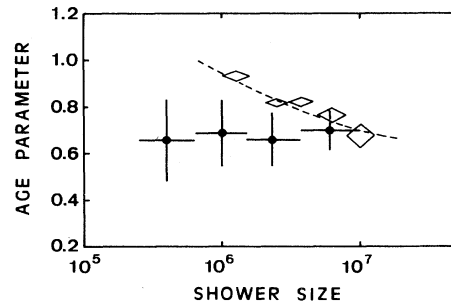


FIG. 12. EAS size dependence of age parameter. Solid circles indicate the mean value with one standard deviation in each size bin for EAS's accompanied by families with $\sum E_{\gamma,H} \geq 10 \text{ TeV}$. Open diamonds indicate the mean value with its probable error for the general EAS. The data at the smallest size are obtained from another experiment (Ref. 10) at Mt. Norikura in 1982.

with errors in 1σ . It keeps well a constant value (~ 0.7) over the size range $(3 \times 10^5) - 10^7$. For the general EAS's, on the other hand, the mean value of this quantity with its probable error (open diamonds) decreases with EAS size in the range up to 10^7 as guided by a dashed line. The data at the smallest size for the general EAS are those obtained from another experiment at Mt. Norikura¹⁰ in 1982. The mean values of s for these two kinds of EAS's agree with each other at the size around 10^7 . Then, this figure shows that the families are associated in general with young EAS's and also suggests that there is little distinction between the two kinds of EAS's in the size region above 5×10^6 .

With the values of attenuation length obtained from the zenith-angle distributions in Fig. 10 we can get the absolute size spectrum of EAS's as shown in Fig. 13. The closed and open marks indicate the data obtained in 1980 and 1981 and in 1985, respectively. The squares indicate the data for the general EAS's, which are represented by a simple power -1.82 . The circles indicate the data for the EAS accompanied by families with $\sum E_{\gamma,H} \geq 10$ TeV. The general EAS spectrum, which seems to extend straight to 10^6 , is free from any detection bias above the size at least 2×10^6 . In the size region larger than a critical size, about 5×10^6 , the EAS's are predominantly accompanied by the families with $\sum E_{\gamma,H} \geq 10$ TeV at the atmospheric depth 738 g cm^{-2} , since both size spectra coincide with each other as seen from this figure. This is quite consistent with the above result obtained from Fig. 12 for the mean-age parameters. The size spectrum of family-associated EAS's, however, drops rapidly from that of the general EAS's as the shower size decreases in the region smaller than the critical size.

This size region is notable because the intensity gap between them is considered to be sensitively affected by the fraction of protons in the primary cosmic rays. In the work by Shima *et al.*¹⁵ a Monte Carlo simulation of both

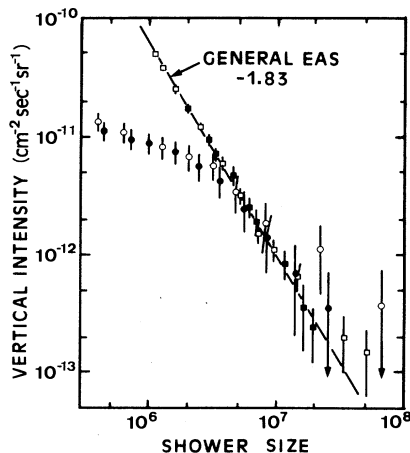


FIG. 13. Integral size spectrum of EAS's. Solid squares (1980 and 1981) and open squares (1985) are for the general EAS and solid circles (1980 and 1981) and open circles (1985) are for the EAS's accompanied by families with $\sum E_{\gamma,H} \geq 10$ TeV.

the family-associated EAS's and the general EAS's is done in order to get the proton fraction in this size region by the comparison with the experimental size spectrum given above. According to their work the proton fraction is given to be $(20 \pm 6)\%$, with an error of 1σ , at the shower size 7×10^5 in the integral size spectrum. This shower size corresponds to the primary energy $(0.9 - 3.3) \times 10^{15}$ eV, with 95% energy spread, in the integral spectrum. This value is compatible with the result $(14 \pm 5)\%$ obtained in Sec. II in this paper from the absolute family intensity within errors.

V. SUMMARY

The results obtained from the simultaneous observation of EAS's and high-energy families are summarized as follows.

The integral $\sum E_{\gamma,H}$ spectrum of families obtained at Mt. Norikura is represented by a simple power -1.3 and its vertical intensity is consistent with the other EX chamber data with $\Lambda_{\text{att}} \approx 100 \text{ g cm}^{-2}$ given by the zenith-angle distribution of these families.

The success rate of the combination between families with $\sum E_{\gamma,H} \geq 10$ TeV and EAS's is close to 90%. The families are associated with young EAS's ($s \sim 0.7$) whose sizes distribute over 3 orders of magnitude up to 10^8 .

The general EAS has a somewhat flat zenith-angle distribution with $\Lambda_{\text{att}} \approx 120 \text{ g cm}^{-2}$, which is consistent with the altitude dependence of its vertical intensity at the size 10^6 .

The size spectrum of the family-associated EAS coincides with the general EAS in the region above the critical size $\sim 5 \times 10^6$, but there is seen a clear gap between them below it.

From the vertical intensity of families, i.e., the $\sum E_{\gamma,H}$ spectrum, the proton fraction in the primary cosmic rays is deduced to be $(14 \pm 5)\%$ with an error of 1σ in the primary energies $(5 \times 10^{14}) - 10^{16}$ eV, in comparison with a Monte Carlo simulation assuming an adequate nuclear interaction model. This agrees with the result obtained by the work¹⁶ with other mountain EX chamber data. This is also compatible with the result inferred from the size spectrum gap, at a designated shower size below the critical one, between the family-associated EAS and the general EAS in comparison with a Monte Carlo simulation.¹⁵

The future problem of this type of experiment is to scale up the EX chamber and to detect more families, especially in higher-energy regions, together with EAS's. Then, one can confirm the present result with respect to the proton fraction obtained from the $\sum E_{\gamma,H}$ spectrum. Moreover, the analysis of the intensity gap of EAS's, mentioned above, for families with higher cutoff energy such as $\sum E_{\gamma,H} \geq 100$ TeV will make it possible to get the energy dependence of the proton fraction in the region $10^{15} - 10^{16}$ eV around the knee in the primary spectrum. There is a plan to construct an EAS detector array and EX chambers in Tibet.²⁹ Further, $\bar{p}p$ data at the Fermilab Tevatron and data of nucleus-nucleus interactions from BNL and CERN will serve to refine the Monte Carlo simulation in the higher-energy region.

ACKNOWLEDGMENTS

The authors would like to express their gratitude to staffs of the Norikura Observatory of the Institute for Cosmic Ray Research, University of Tokyo for continu-

ous support of the experiment. The EAS data was processed in the Computer Center of Konan University by HITAC M-260 D. This work was supported by a Grant in Aid for Scientific Research from the Ministry of Education, Science and Culture.

- ¹Yu. A. Smorodin *et al.*, in *Proceedings of Ninth International Conference on Cosmic Rays*, London, England, 1965, edited by A. C. Stickland (The Institute of Physics and The Physical Society, London, 1965), Vol. 2, p. 827.
- ²S. Dake *et al.*, *Acta Phys. Hung.* **29**, Suppl. 3, 671 (1970).
- ³T. Matano *et al.*, *Acta Phys. Hung.* **29**, Suppl. 3, 451 (1970).
- ⁴S. Dake *et al.*, *Nuovo Cimento B* **41**, 55 (1977).
- ⁵M. Sakata *et al.*, *Nuovo Cimento A* **70**, 3 (1982); **70**, 297 (1982).
- ⁶H. Munakata *et al.*, *J. Phys. G* **6**, 1575 (1980).
- ⁷UA5 Collaboration, G. J. Alner *et al.*, *Phys. Lett.* **167B**, 476 (1986).
- ⁸Y. Fukushima *et al.*, in *Proceedings of the Nineteenth International Cosmic Ray Conference*, La Jolla, California, 1985, edited by F. C. Jones, J. Adams, and G. M. Mason (NASA Conf. Publ. 2376) (Goddard Space Flight Center, Greenbelt, MD, 1985), Vol. 7, p. 73; *Memoirs of Konan University*, Science Series (Konan University, Kobe, Japan, 1987), Vol. 34, p. 207.
- ⁹K. Kamata and J. Nishimura, *Suppl. Prog. Theor. Phys.* **6**, 142 (1958).
- ¹⁰To. Saito *et al.*, in *Eighteenth International Cosmic Ray Conference, Bangalore, India, 1983, Conference Papers*, edited by N. Durgaprasad *et al.* (Tata Institute of Fundamental Physics, Bombay, 1983).
- ¹¹C. M. G. Lattes *et al.*, in *Proceedings of the Thirteenth International Conference on Cosmic Rays*, Denver, 1973 (Colorado Associated University Press, Boulder, 1973), Vol. 3, p. 2219.
- ¹²V. K. Budilov *et al.*, in *Proceedings of the Fourteenth International Conference on Cosmic Rays*, Munich, 1975, edited by Klaus Pinkau (Max-Planck-Institut, München, 1975), Vol. 7, p. 2365.
- ¹³J. R. Ren *et al.*, in *Eighteenth International Cosmic Ray Conference, Bangalore, India, 1983, Conference Papers* (Ref. 10), Vol. 11, p. 118.
- ¹⁴M. Amenomori *et al.*, in *Eighteenth International Cosmic Ray Conference, Bangalore, India, 1983, Conference Papers* (Ref. 10), Vol. 11, p. 110.
- ¹⁵M. Shima *et al.*, following paper, *Phys. Rev. D* **39**, 1275 (1989).
- ¹⁶J. R. Ren *et al.*, *Phys. Rev. D* **38**, 1404 (1988).
- ¹⁷T. Shirai *et al.*, in *Proceedings of International Cosmic Ray Symposium on High Energy Physics*, Tokyo, 1974, edited by A. Ohsawa and T. Yuda (Institute for Cosmic Ray Research, University of Tokyo, Tokyo, 1974), p. 39.
- ¹⁸S. Hayakawa *et al.*, *Suppl. Prog. Theor. Phys.* **32**, 104 (1964).
- ¹⁹BASJE Collaboration, F. Kakimoto *et al.*, in *Proceedings of the Seventeenth International Cosmic Ray Conference*, Paris, France, 1981 (CEN-Saclay, Gif-sur-Yvette, 1981), Vol. 11, p. 254; K. Suga, *Sixteenth International Cosmic Ray Conference, Kyoto, 1979, Conference Papers* (Institute of Cosmic Ray Research, University of Tokyo, Tokyo, 1979), Vol. 14, p. 325.
- ²⁰Tien Shan Collaboration, S. K. Machavariani *et al.*, *Sixteenth International Cosmic Ray Conference, Kyoto, 1979, Conference Papers* (Ref. 19), Vol. 8, p. 240.
- ²¹OCU Collaboration, S. Miyake *et al.*, *J. Phys. Soc. Jpn.* **16**, 847 (1961).
- ²²OCU Collaboration, S. Miyake *et al.*, in *Proceedings of the Twelfth International Conference on Cosmic Rays*, Hobart, 1971, edited by A. G. Fenton and K. B. Fenton (University of Tasmania Press, Hobart, Tasmania, 1971), Vol. 7, p. 2748.
- ²³Akeno Collaboration, K. Kamata *et al.*, in *Proceedings of the Seventeenth International Cosmic Ray Conference* (Ref. 19), Vol. 13, p. 305.
- ²⁴Moscow Collaboration, G. B. Christiansen *et al.*, in *Proceedings of the Ninth International Conference on Cosmic Rays* (Ref. 1), Vol. 2, p. 799.
- ²⁵Tokyo INS Collaboration, S. Fukui *et al.*, *Prog. Theor. Phys. Suppl.* **16**, 1 (1960).
- ²⁶Kobe Collaboration, K. Asakimori *et al.*, *Sixteenth International Cosmic Ray Conference, Kyoto, 1979* (Ref. 19), Vol. 8, p. 252.
- ²⁷Lodz Collaboration, Ph. Catz *et al.*, in *Proceedings of the Fourteenth International Cosmic Ray Conference* (Ref. 12) Vol. 12, p. 4329.
- ²⁸Durham Collaboration, W. S. Rada *et al.*, in *Proceedings of the Fifteenth International Conference on Cosmic Rays*, Plovdiv, 1977, edited by B. Betev (Bulgarian Academy of Science, Plovdiv, Sofia, 1977), Vol. 8, p. 13.
- ²⁹J. R. Ren *et al.*, in *Proceedings of International Symposium on Cosmic Ray Superhigh Energy Interactions*, Beijing, 1986, edited by L. K. Ding, H. H. Kuang, and J. R. Ren (Institute of High Energy Physics, Academia Sinica, 1986), p. 9-13.